Journal of Power Sources 248 (2014) 343–347

Contents lists available at ScienceDirect

Journal of Power Sources

journal homepage: www.elsevier.com/locate/jpowsour

Short communication

Polythiophene coordination complexes as high performance lithium storage materials

Ya Mao [a,c], Qingyu Kong [b,**], Lian Shen [a], Zhaoxiang Wang [a,*], Liquan Chen [a]

[a] Key Laboratory for Renewable Energy, Beijing Key Laboratory for New Energy Materials and Devices, Beijing National Laboratory for Condensed Matter Physics, Institute of Physics, Chinese Academy of Sciences, P.O. Box 603, Beijing 100190, China
[b] Société Civile Synchrotron SOLEIL, L'Orme des Merisiers, Saint-Aubin-BP 48, GIF-sur-YVETTE Cedex 91192, France
[c] Shanghai Institute of Space Power-Sources (SISP), Shanghai Academy of Spaceflight Technology, Shanghai 200045, China

HIGHLIGHTS

- Polythiophene-based coordination complexes were synthesized by chemical method.
- PTh–Fe and PTh–Fe–O composites are novel promising lithium storage materials.
- The coordination between Fe and PTh ensures high capacity and stable cyclability.

ARTICLE INFO

Article history:
Received 20 June 2013
Received in revised form
20 August 2013
Accepted 4 September 2013
Available online 27 September 2013

Keywords:
Polythiophene
Coordination
Lithium storage
Lithium ion batteries

ABSTRACT

Polythiophene (PTh)-based coordination complexes, polythiophene–iron (PTh–Fe) and polythiophene–iron–oxygen (PTh–Fe–O) were synthesized by chemical method and proved to be novel high-performance organometallic lithium-storage materials. Extended X-ray absorption fine structural (EXAFS) spectroscopy and density functional theory (DFT) calculations indicate that these complexes have layered structures. It is believed that the strong and stable Fe–S coordination creates sites of lithium storage and ensures the high specific capacity and outstanding cycle performance of the PTh-based complexes.

1. Introduction

Conducting polymers have attracted considerable interest in recent years due to their high intrinsic conductivity, environmental stability and wide applications in different technologies such as electrochemical displays, sensors, and redox capacitors. Although these conducting polymers can be used both as anode (by exploiting their reduction or *n*-doping process) and cathode (by oxidation or *p*-doping process), most of their applications are confined to battery cathodes, with capacities between 80 and 90 mAh g^{-1} above 2.0 V *vs.* Li^+/Li [1]. The mechanism of the redox reaction is anion ingress/egress. The lithium storage capacities of these polymers are negligible below 2.0 V.

Polythiophene (PTh) and its derivatives are considered as appropriate cathode materials and conducting additives for secondary lithium batteries [2–4], mainly due to their high working potentials, and stability to undergo both *n*- and *p*-doping. In a Li/$LiClO_4$-PC/PTh cell [5], PTh electrode synthesized by electrochemical polymerization shows high working potential (~3.3 V) and coulombic efficiency. However, its specific capacity is only 30 mAh g^{-1}. The chemically synthesized PTh powder exhibits specific capacities from 20 to 50 mAh g^{-1} and an average potential of 3.6 V [6,7].

Recently, we found that chemically or electrochemically synthesized PPy–M–O (M = Fe, Co, Ni; PPy for polypyrrole) coordination complexes could be used as high-performance lithium-storage materials [8–10]. The strong metal-polymer interaction decreases the strength of some chemical bonds on the polymer and makes them new sites for lithium storage.

In this work, PTh-based coordination complexes (PTh–Fe and PTh-Fe-O) were synthesized by chemical polymerization, and

* Corresponding author. Tel./fax: +86 10 8265 9050.
** Corresponding author. Tel.: +33 (0)1 6935 9784.
E-mail addresses: kong@synchrotron-soleil.fr (Q. Kong), zxwang@iphy.ac.cn (Z. Wang).

0378-7753/$ – see front matter © 2013 Elsevier B.V. All rights reserved.
http://dx.doi.org/10.1016/j.jpowsour.2013.09.019

evaluated as lithium storage materials. It will be seen that the coordination between Fe and PTh ensures the high specific capacity and stable cyclability of these layer-structured complexes as anode materials for lithium ion batteries.

2. Experimental

The PTh–Fe composite was prepared by a chemical polymerization method with anhydrous $FeCl_3$ (Beijing Chemicals) as the oxidant. In a typical experiment, 10 mmol thiophene monomer (A.R., Beijing Mashi Fine Chemicals) was taken in a flask containing 40 ml $CHCl_3$ (Beijing Chemicals). Then 16.7 mmol $FeCl_3$ in 80 ml $CHCl_3$ solution was added. The mixture was mechanically stirred for 24 h at room temperature. The product was washed with ethanol several times before dried at 50 °C under vacuum for 24 h to obtain brown powder, PTh–Fe. The PTh–Fe–O composite was prepared by the same method except that commercial nano-CuO powder (Alfa, 23–37 nm in size) was added as an auxiliary.

Electrochemical evaluation and physical characterization were conducted as described in our previous reports [8–10]. In short, electrodes were prepared by mixing the as-prepared powder (80 wt.%), carbon black (10 wt.%) and polyvinylidene fluoride (PVDF; 10 wt.%) binder. With fresh lithium foil as the counter electrode, 1 mol L^{-1} $LiPF_6$ dissolved in a mixture of ethylene carbonate (EC) and dimethyl carbonate (DMC) (1:1 v/v) as the electrolyte, and Celgard 2400 as the separator, test cells were assembled in an Ar-filled glove box (MBraun, Lab Master 130). The cell was galvanostatically cycled between 0.0 and 3.0 V *vs.* Li^+/Li at a current density of 0.1 mA cm^{-2}.

XAS spectra were measured at the Fe and Cl *k*-edges in fluorescence mode at LUCIA beamline SOLEIL Synchrotron. Briefly, the X-ray was produced from the APPLE-II undulator (UE54) with a source size of 200 × 20 μm^2 (H × V, FWHM), then focused by a spherical mirror onto two flat mirrors which act as low-pass filters to reject the high-order harmonics from the undulator and reduce the thermal load on the monochromator. A Si(111) double crystal monochromator (DCM) is used to obtain the XAS spectra with an angular scanning range from 5 to 75°. After the monochromator, a Kirkpatrick-Baez (KB) mirror is used to focus the X-ray on the sample with a spot size of 2.5 × 2.5 μm^2 and flux of 1012 photons/s. The sample was prepared and glued to the sample holder in an argon-filled glove box and sealed with Krypton foil, then put in the sample vacuum chamber at LUCIA beamline. A mono-element energy dispersive silicon drift diode (SDD) mounted perpendicular to the incident X-ray beam is used to collect the fluorescence emission from the sample. The distance between the SDD detector and the sample is 20 cm [11].

3. Results and discussion

The PTh-Fe powder (Fig. 1a) appears as aggregated particles of around 200 nm. Thermogravimetric analysis (TGA) (Fig. 1b) demonstrates that the mass loss of the PTh-Fe and PTh-Fe-O composites is around 80% and 36% at 800 °C, indicating that the content of PTh in the PTh–Fe and PTh–Fe–O is 80 and 36 wt.%, respectively. Elemental analysis by inductively coupled plasma (ICP) technique shows that the content of S and Fe in the PTh–Fe composite is 25.4 and 8.91 wt.%, and the content of S, Fe and Cu in the PTh–Fe–O composite is 13.0, 27.4 and 0.66 wt.%, respectively. The content of Cu is negligible in the composite as the auxiliary CuO was dissolved in the acidic $FeCl_3$ solution during material preparation.

The Raman spectrum of the PTh–Fe–O composite is very similar to that of the PTh–Fe composite (Fig. 1c). The C=C asymmetric and symmetric stretch vibrations of the thiophene ring appear at 1494 and 1454 cm^{-1}, respectively [12,13]. The peak at 1216 cm^{-1} is attributed to the C–C stretching. The band of C_β–H bending

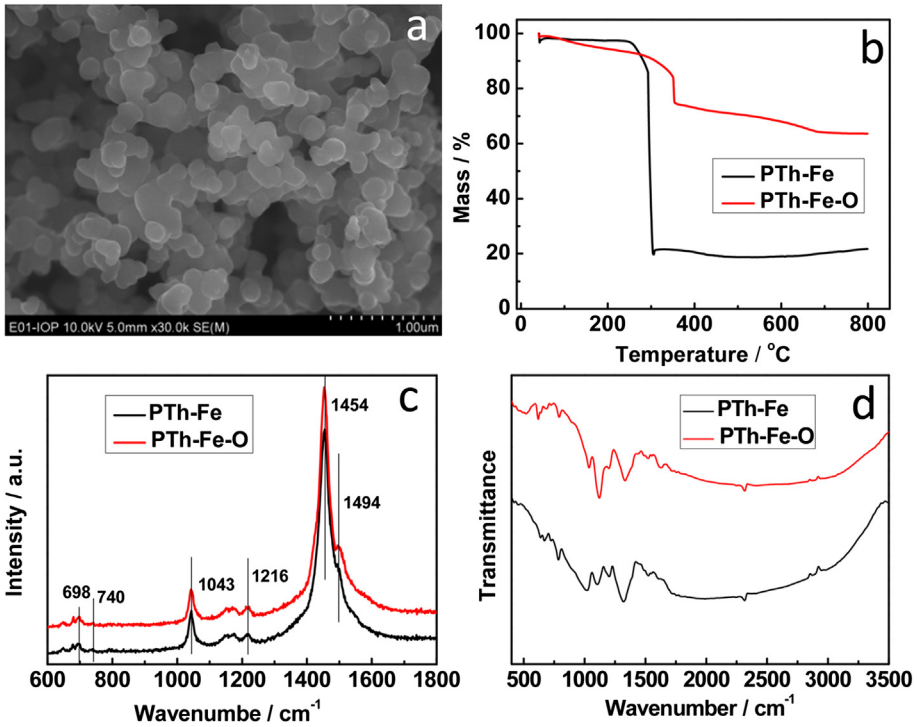

Fig. 1. The morphology of the PTh–Fe composite (a) and the TGA between room temperature and 800 °C in the oxygen atmosphere at a scan rate of 10 °C min. (b), Raman (c), and FTIR (d) spectra of the PTh–Fe and PTh–Fe–O composites.

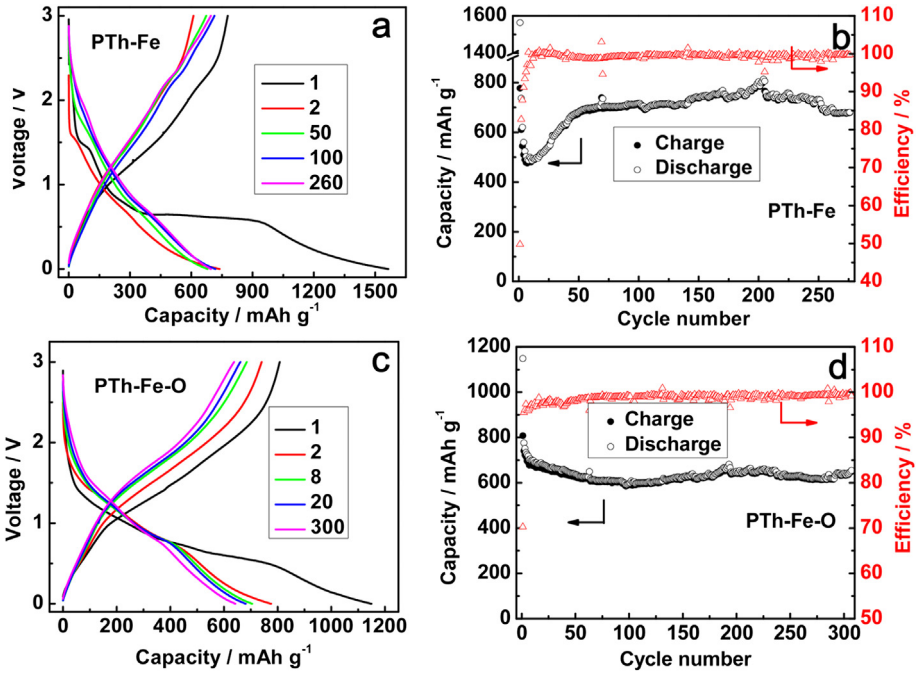

Fig. 2. The electrochemical performance of the PTh–Fe and PTh–Fe–O composites between 0.0 V and 3.0 V *vs.* Li^+/Li: selected potential profiles of PTh–Fe (a) and PTh–Fe–O (c); the galvanostatic cycling performance of the PTh–Fe (b) and PTh–Fe–O (d) composites, at a current density of 0.1 mA cm^{-2}.

appears at 1043 cm^{-1}. The peaks at 740 and 698 cm^{-1} are related to the ring deformation of C–S–C. Most of these peaks are identical with the calculated and experimental results of thiophene [14].

The FTIR spectra of the PTh–Fe and PTh–Fe–O composites are shown in Fig. 1d. The two peaks at 1486 and 1451 cm^{-1} belong to the C=C asymmetric and symmetric stretching of the thiophene ring, respectively [15]. The strong peak at 1320 cm^{-1} is attributed to the C–C stretching [14]. The bands at 1102 cm^{-1} and 1023 cm^{-1} can be assigned to the in-plane C_β–H aromatic bending [13,16,17]. The peak at 785 cm^{-1} is attributed to the out-of-plane C_β–H aromatic bending of the thiophene ring, indicating the α-position linkage between the thiophene rings, whereas the peaks at 668 and 638 cm^{-1} are indicative of the C–S stretching of the thiophene ring [13,15,18]. The presence of these characteristic peaks confirms the formation of the PTh with a 2, 5-substituted thiophene ring.

The voltage profiles of the PTh–Fe and PTh–Fe–O composites between 0.0 V and 3.0 V are shown in Fig. 2. The reversible capacity of the PTh–Fe composite in the first cycle is 776 mAh g^{-1} and the coulombic efficiency is 50%. Similarly, the initial reversible capacity of the PTh–Fe–O composite is 808 mAh g^{-1} and its coulombic

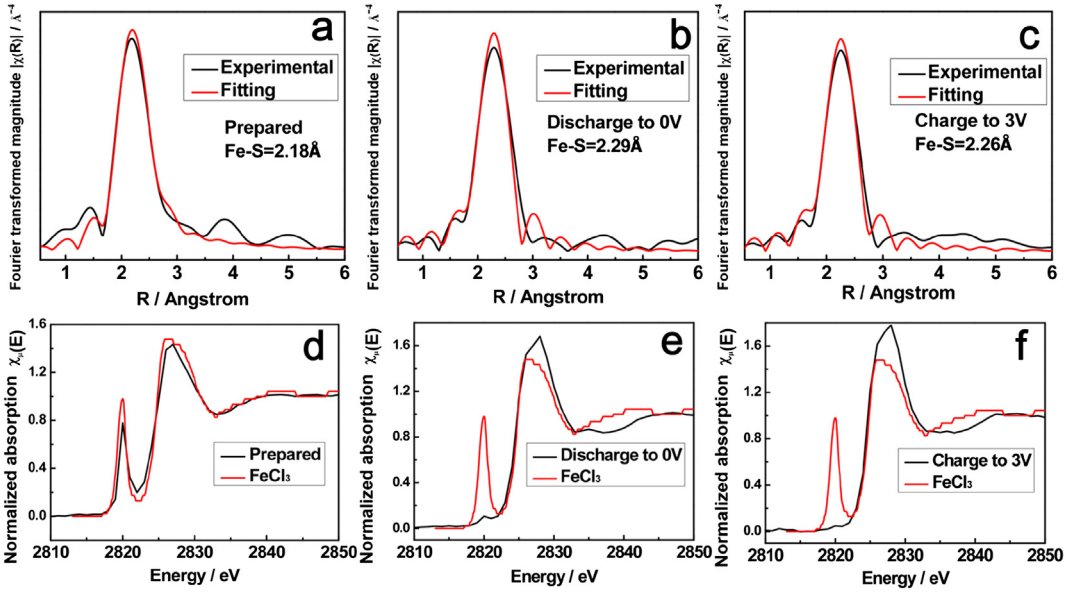

Fig. 3. The experimental (black) EXAFS signals at the Fe *k*-edge (a–c) and XANES spectra at Cl *k*-edge (d–f) of the PTh–Fe composite at various states: as-prepared (a, d), discharged to 0.0 V (b, e) and recharged to 3.0 V (c, f). The red lines in (a–c) are for the DFT fitting results based on a monolayer structure while the red curves in (d–f) are for the Cl *k*-edge XANES spectrum of $FeCl_3$ for reference. (For interpretation of the references to color in this figure legend, the reader is referred to the web version of this article.)

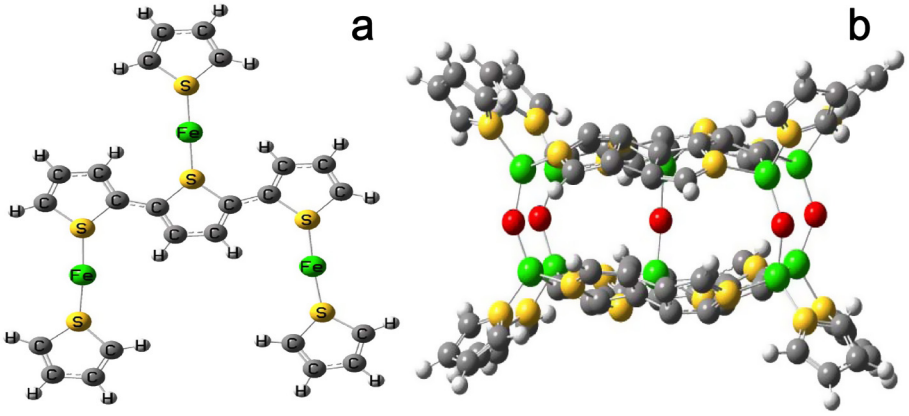

Fig. 4. The experimental (black) EXAFS signals at the Fe *k*-edge (a–c) and XANES spectra at Cl *k*-edge (d–f) of the PTh–Fe–O composite at various states: as-prepared (a, d), discharged to 0.0 V (b, e) and recharged to 3.0 V (c, f). The red lines in (a–c) are for the DFT fitting results based on two-layer structure while the red curves in (d–f) are for the Cl *k*-edge XANES spectrum of $FeCl_3$ for reference. (For interpretation of the references to color in this figure legend, the reader is referred to the web version of this article.)

efficiency is around 71%. The capacities of the PTh–Fe and PTh–Fe–O composites are about 650 mAh g^{-1} after 300 cycles. Compared to the low capacity of pure PTh, only 80 mAh g^{-1} above 2.0 V [1] and negligible below 2.0 V, the high capacity of the PTh–Fe or PTh–Fe–O composite is believed to originate from some different lithium storage mechanisms.

Based on our earlier studies on PPy coordination complexes, such as PPy–Fe–O, PPy–Co–O and PPy–Ni–O [8–10], a similar lithium storage mechanism is proposed for the present PTh–Fe and PTh–Fe–O composites. The strong coordination between Fe or Ni and N of PPy weakens the C–H bonds in the C_4N ring framework, permitting them possess high lithium storage capacity. Similarly, the coordination between Fe and S in the thiophene unit of *t* results in the high-performance lithium storage of the PTh–Fe and PTh–Fe–O composites. This assumption is confirmed by the EXAFS and XANES analysis of the PTh–Fe and PTh–Fe–O composites at various discharged/recharged states.

DFT fitting to the experimental EXAFS signal of the prepared PTh–Fe sample at the Fe *k*-edge (Fig. 3) illustrates the co-existence of the monolayered PTh–Fe complex and other forms of Fe in the as-prepared sample. The XANES spectra at Cl *k*-edge (Fig. 3d) of the as-prepared sample shows a strong pre-peak around 2820 eV, which comes from $FeCl_3$ with a high symmetric structure (space group R3-H) as illustrated with the XANES spectrum of $FeCl_3$. Our result indicates that a small amount of the residual $FeCl_3$ from the oxidant exists in the prepared sample. The linear combination data analysis produced a molar ratio of 85% for PTh–Fe complex with one layer structure and 15% for $FeCl_3$ in the prepared sample. The layered structure of the PTh–Fe complex in Fig. 4a is calculated from the DFT with B3LYP/6-31G(d) method based on which the theoretical EXAFS signals in Fig. 3a–c are simulated. In this configuration, each Fe atom is coordinated with two S atoms in the thiophene units, forming S–Fe–S chemical bonds in a layer-like PTh–Fe network. Data fitting shows that the Fe–S distance is 2.18 Å. The strong coordination between Fe and S of the thiophene weakens the C–H and C–C bonds in the thiophene ring framework, making them a hydrogen-deficient Fe–C_4S network for lithium storage over or under the rings. The fitting results of the EXAFS signals at the Fe *k*-edge show that the one layer structure remains stable both at the discharged and recharged samples, with the Fe–S

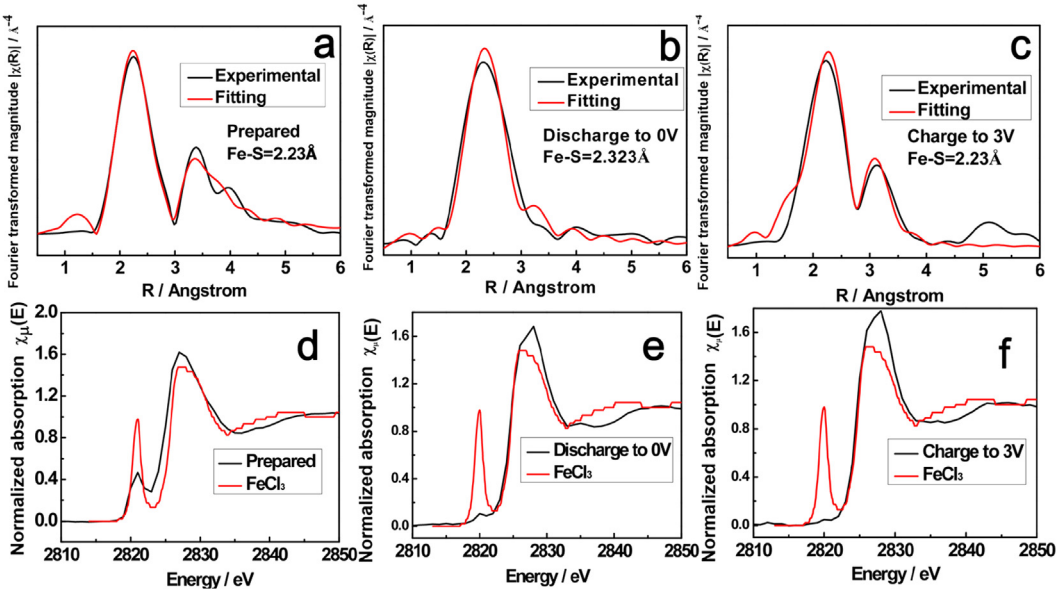

Fig. 5. The DFT-calculated structure of PTh–Fe (a) and PTh–Fe–O (b) coordination complexes based on the EXAFS results (Figs. 3a and 4a, respectively).

distances changed to 2.29 Å and 2.26 Å at discharged (0.0 V) and recharged (3.0 V) states.

As the XANES spectra at Cl *k*-edge show in Fig. 3e and f, the strong pre-peak at 2820 eV disappears, indicating that no $FeCl_3$ exists in the discharged and recharged samples.

Similar to the PTh–Fe composite, the appearance of the pre-peak at 2820 eV of the XANES spectra at the Cl *k*-edge (Fig. 5) indicates that trace amount of $FeCl_3$ co-exists in the as-prepared PTh–Fe–O composite. The experimental absorption coefficient $k\chi(k)$ and Fourier transformed magnitude $|\chi(R)|$ of the prepared PTh–Fe–O composite is fitted with a linear combined signal from $FeCl_3$ and two-layer PTh–Fe–O. The linear combination data analysis produced a molar ratio of 95% for PTh–Fe–O two-layer structure and 5% for $FeCl_3$ in the prepared sample. No $FeCl_3$ remains in the discharged and recharged samples, as shown by the XANES spectra at Cl *k*-edge in Fig. 5e and f.

In the two-layer structured PTh–Fe–O coordination complex (Fig. 4b), the Fe is incorporated into the PTh matrix, forming S–Fe–S chemical bonds in a layer-like PTh–Fe network, and the two neighboring layers are connected by the Fe–O–Fe interactions.

When the cell is discharged to 0.0 V, the fitting results of the Fourier transformed magnitude $|\chi(R)|$ at Fe *k*-edge (Fig. 5b) shows that the two-layer structure of the PTh–Fe–O complex was destroyed to PTh–Fe one layer structure. The Fe–O–Fe interaction between layers in the prepared sample is broken, only the one layer structure with Fe incorporated into the PTh network exists in the discharged sample, with Fe–S distance of 2.323 Å. After recharged to 3.0 V, the fitting results show that the two-layer structure of the PTh–Fe–O complex is reformed, with an Fe–S distance of 2.23 Å. The strong and stable Fe–S coordination weakens the C–H and C–C bonds of the thiophene units and ensures the high specific capacity of the PTh–Fe–O complex. The high reversibility of its interlayer Fe–O–Fe interaction during cycling permits its high cycling stability.

4. Conclusions

PTh–Fe and PTh–Fe–O composites were synthesized by chemical method. Electrochemical evaluation revealed that these PTh-based composites are novel promising lithium storage materials with a reversible capacity over 700 mAh g^{-1} and excellent cycling stability for over 300 cycles. The strong and stable Fe–S coordination ensures the high specific capacity. The previously reported PPy-based complexes [8–10] and the current PTh-based complexes are actually novel types of lithium storage materials, which pave new ways to construct high-performance organic anode materials for lithium ion batteries. These complexes are expected to find wide applications in supercapacitors, high-efficiency and inexpensive electrocatalysts for fuel cells, *etc*.

Acknowledgments

This work was financially supported by the National 973 Program (2009CB220104) and the National Science Foundation of China (NSFC, No. 50472072 and 20974120). We are grateful to Pierre Lagarde from LUCIA beamline at Soleil for XAS data collection and analysis.

References

[1] P. Novák, K. Müller, K.S.V. Santhanam, O. Haas, Chem. Rev. 97 (1997) 207–282.
[2] F. Wu, S. Wu, R. Chen, J. Chen, S. Chen, Electrochem. Solid-State Lett. 13 (2010) A29–A31.
[3] F. Wu, J. Chen, R. Chen, S. Wu, L. Li, S. Chen, T. Zhao, J. Phys. Chem. C 115 (2011) 6057–6063.
[4] G.R. Goward, F. Leroux, L.F. Nazar, Electrochim. Acta 43 (1998) 1307–1313.
[5] H.Y. Yang, W. Jiang, Y. Lu, Mater. Lett. 61 (2007) 1439–1442.
[6] K. Ryu, Mater. Chem. Phys. 84 (2004) 380–384.
[7] L. Liu, F. Tian, X. Wang, Z. Yang, M. Zhou, X. Wang, React. Funct. Polym. 72 (2012) 45–49.
[8] Y. Mao, Q.Y. Kong, B.K. Guo, X.P. Fang, X.W. Guo, L. Shen, M. Armand, Z.X. Wang, L.Q. Chen, Energy Environ. Sci. 4 (2011) 3442–3447.
[9] B.K. Guo, Q.Y. Kong, Y. Zhu, Y. Mao, Z.X. Wang, M.X. Wan, L.Q. Chen, Chem. Eur. J. 17 (2011) 14878–14884.
[10] Y. Mao, Q.Y. Kong, B.K. Guo, L. Shen, Z.X. Wang, L.Q. Chen, Electrochim. Acta 105 (2013) 162–169.
[11] A.M. Flank, G. Gauchon, P. Lagarde, S. Bac, M. Janousch, R. Wetter, J.M. Dubuisson, M. Idir, F. Langlois, T. Moreno, D. Vantelon, Nucl. Instum. Methods B 246 (2006) 269–274.
[12] G. Ceder, B. Kang, J. Power Sources 194 (2009) 1024–1028.
[13] M.R. Karim, C.J. Lee, M.S. Lee, J. Polym. Sci. Part A: Polym. Chem. 44 (2006) 5283–5290.
[14] M. Lubbe, A.M. Gigler, R.W. Stark, W. Moritz, Surf. Sci. 604 (2010) 679–685.
[15] M. Lu, S. Yang, Synth. Met. 154 (2005) 73–76.
[16] A. Gok, M. Omastova, A. Yavuz, Synth. Met. 157 (2007) 23–29.
[17] X.-G. Li, J. Li, M.-R. Huang, Chem. Eur. J. 15 (2009) 6446–6455.
[18] A. Uygun, A.G. Yavuz, S. Sen, M. Omastova, Synth. Met. 159 (2009) 2022–2028.